JOURNAL OF MATERIALS RESEARCH AND TECHNOLOGY 2021;15:5948–5967

Available online at www.sciencedirect.com

jmr&t Journal of Materials Research and Technology

journal homepage: www.elsevier.com/locate/jmrt

Original Article

Lateral friction surfacing: experimental and metallurgical analysis of different aluminum alloy depositions

*Ebrahim Seidi**, *Scott F. Miller*

Department of Mechanical Engineering, University of Hawaii at Manoa, Honolulu, HI, USA

ARTICLE INFO

Article history:
Received 28 August 2021
Accepted 9 November 2021
Available online 13 November 2021

Keywords:
Solid-state deposition
Material processing
Infrared thermography
Characterization
SEM
EDS

ABSTRACT

Lateral friction surfacing, a solid-state deposition process, is a novel friction surfacing technique. In this approach, frictional heat and plastic deformation result in deposition of consumable material from the radial surface of a tool onto a substrate. This paper presents a comprehensive assessment of lateral friction surfacing of AA2011, AA6061, and AA7075 aluminum alloys, with particular focus on the impacts of process parameters on the coating properties. The influence of process variables such as tool rotational speeds, normal applied forces, and type of consumable materials was investigated on the process temperature, physical, and metallurgical characteristics of the deposits using optical microscopy, infrared thermography, scanning electron microscopy, and EDS. This study exhibits that the lateral friction surfacing approach enables the deposition of ultra-thin and smooth layers of different aluminum alloys. Furthermore, the temperature generated in this technique was low enough to avoid plasticizing the substrate and intermixing between the consumable material and substrate, which mitigates the thermal impacts on the grain structures and metallurgical characteristics. The lateral friction surfacing performance of the different alloys can be partially explained by their material properties. High input energy provided by high normal forces and tool rotational speeds may result in failure in the deposition process of materials with lower thermal conductivity and melting point, which emphasizes on limitations for the process parameters during the process.

1. Introduction

Friction surfacing (FS) is a friction based solid-state additive manufacturing technique for transfer of one material onto a substrate [1]. This technique allows the bonding of similar and dissimilar metallic material combinations. In this technique, the rotating consumable rod is forced against the surface of a substrate, as shown in Fig. 1. Frictional heat is generated at the contact interface of the substrate and consumable rod, which facilitates the softening and shearing of consumable material [1]. The material is deposited in a viscoplastic layer at the interface of the rod and substrate, which creates a bond between the coating layer and the workpiece. This technique is capable of providing high-quality bonding with lower deformation in a wide variety of materials. Compared to the fusion-

* Corresponding author.
E-mail address: seidi@hawaii.edu (E. Seidi).

https://doi.org/10.1016/j.jmrt.2021.11.049

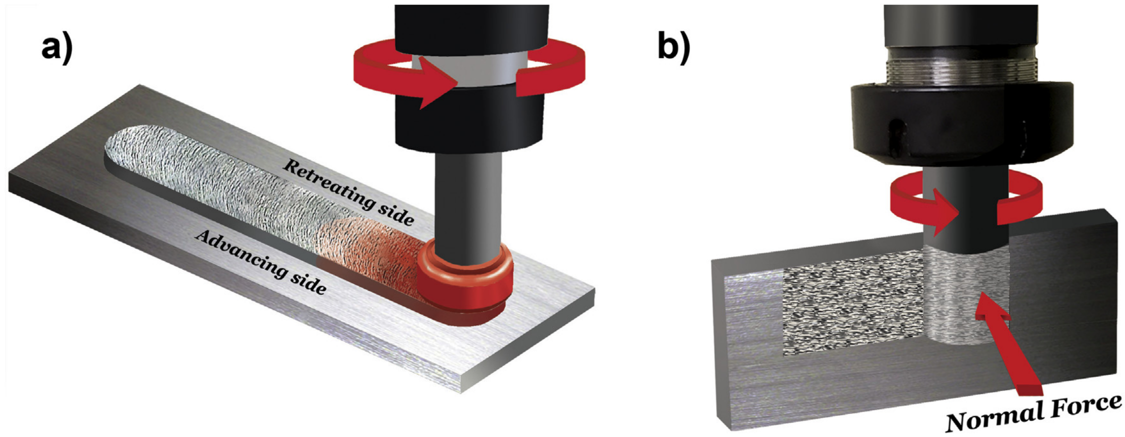

Fig. 1 – FS using (a) the end of the consumable tool (b) the radial surface of the consumable tool.

based methods, the solid-state substance of FS and the lower input energy during the process result in a reduced heat affected zone (HAZ) and limits large distortion issues [2]. The FS technique is basically an environmentally friendly process since shielding gas and forced cooling methods are not necessarily required in this approach.

The effective process parameters in this technique comprise a wide range of factors such as material properties including physical properties (surface roughness, melting point), thermo-mechanical properties (shear and yield strength, hardness, and thermal conductivity), process conditions (length and diameter of the rod, thickness and size of the substrate, and atmosphere), as well as other factors such as tool rotational speed, applied force, and transverse speed. All these process parameters influence the coating properties such as thickness, hardness, surface roughness, and bond strength [3]. The impacts of critical process factors such as spindle speed, axial force, table traverse speed [4–6], tool diameter [7–9], single and multiple layer deposition [10], different tool configuration [11], and different material types [12–17] on the coating quality have been studied in various investigations. Many investigations have been conducted to study the influence of process parameters on process temperature [18–20], residual stress [21,22], width and thickness [23], wear resistance performance [24,25], surface roughness [26], hardness [27,28], corrosion [29,30], bond strength [31,32], and microstructures [16,33,34].

There is a need for investigations that focus on FS using different combinations of tool/substrate material, with particular attention to the effects of alloys' compositions on the results of this technique to make this approach legitimately possible in industrial applications. Batchelor et al. investigated multi-layer FS of aluminum, brass, and stainless steel onto a mild steel substrate by employing different process parameters and nitrogen shielding gas [13]. In this study, a thick layer of stainless steel was fabricated on the substrate; however, the technique was unsuccessful for brass and aluminum. In another study [35], the different weight percentages of Ag powder were added to AA2024 consumable tools to provide different alloys of this material. It was revealed that by increasing 1 wt.% Ag powder, the strength and hardness of the deposits improved approximately by 1.8 and 1.0 percent, respectively. In another investigation by Shariq et al. [36], AISI 304 stainless steel and copper as consumable tools and mild steel, AISI 304 stainless steel, AA1050, and copper as substrates were examined. In this study, the FS of stainless steel onto copper was not successful, since copper was not able to tolerate the high process temperature. This results in failure of the process, which indicates the importance of process parameters optimization in this technique.

Friction deposition of H13 tool steel onto the surface on a low carbon steel substrate was investigated by Rafi et al. [37]. In this study, the traverse speed and spindle speed were considered as the process variables, while the axial load was kept constant. It was concluded that the deposit's width was bigger than the tool diameter for all the traverse speed employed in the study. Also, the experiment results revealed that the coating width was noticeably decreased by applying higher tool rotational speeds; however, the traverse speed did not have a significant effect on the coating width. An attempt was made in [38] to determine an appropriate set of process factors for FS of a mild steel substrate with 6063 aluminum alloy. The result of the study exhibited that applying higher forging force decreases the coating thickness. On the other hand, FS of Monel 500 onto AISI 1012 steel showed that increasing the axial forging force resulted in higher coating thickness and width [39].

Friction deposition of AA6063 consumable tool onto AISI316 stainless steel substrate and the correlation of the process parameters with the coating geometry were investigated by Sahoo et al. [40]. In this study, three different values for each critical process parameters of traverse speed, axial load, and spindle speed were employed, and their influence on the coating width and thickness were evaluated. It was exhibited that decreasing the tool rotational speed and increasing the axial load results in wider coatings. Also, lower coating thickness values were achieved as the axial load and tool rotational speed were increased. In another investigation [41], stainless steel 316L was friction surfaced onto 304 stainless steel substrates. It was revealed that increasing the spindle speed causes a decrease in both coating thickness and width. Fitseva et al. employed different spindle speeds of 400, 600, 3000, and 6000 rpm to deposit Ti–6Al–4V onto Ti–6Al–4V substrate using FS technique. Their investigation revealed that rougher deposits were obtained using higher tool rotational speeds, and lower tool rotational speeds results in a smoother deposit [42].

FS is a metal deposition approach in which the material transfer occurs at a temperature lower than the melting point of the consumable material. Moreover, the deposited material experiences an intense cooling rate after the process, which results in a fine-grained deposit. Therefore, the process temperature plays a critical role in the FS approach and may change the metallurgical properties of the deposited coating. The heat input can be controlled by the process variables such as tool rotational speed, traverse speed, axial load, and substrate surface roughness. Sekharbabu et al. utilized the FS technique to create a coating layer of D2 tool steel onto a low carbon steel substrate [43]. In this investigation, the microstructures were evaluated using optical microscopy, SEM, and X-ray diffraction. The process temperature profile was provided by means of an infrared camera, and the highest process temperature was recorded as about 1200 °C. The result of SEM analysis exhibited that the carbides present in the coating are finer compared to the as-received D2 consumable tool due to the severe plastic deformation. Puli and Ram investigated and compared the deposited coatings of AISI 410 stainless steel provided by two different approaches of FS and manual metal arc welding [44]. The study result revealed no dilution in the FS process as an advantage for this approach. All of the aforementioned research was done for FS from the end of the tool as shown in Fig. 1(a). There is a lack of research in FS from the radial surface of the tool, as shown in Fig. 1(b), which is addressed in the current study.

A novel method of FS entitled lateral friction surfacing (LFS) was employed in [45], in which the lateral surface of the consumable tool was forced against the surface of the substrate, and material transferring occurred from the side of the tool, as shown in Fig. 1(b). In this study, AISI 1018 carbon steel and AA6063 were employed as the materials of the substrate and consumable tool, respectively. The experimental results of the novel approach revealed that the LFS approach is capable of producing multi-pass deposition with ultra-thin and smooth coating in which the surface roughness values were in the order of 1 μm. This technique generated a lower process temperature compared to the conventional FS technique, and the coating deposited in this approach exhibited

Table 1 – Chemical composition and physical properties of AA6061-T6.

Materials	Mg	Si	Cu	Cr	Mn	Ti	Zn	Fe	Al
% of composition	0.8–1.2	0.4–0.8	0.15–0.4	0.04–0.35	0.15	0.15	0.25	0.7	Balance
Physical Property	Melting Point		UTS	Elongation at Break in 50 mm				Thermal Conductivity	
Values	588 °C		310 MPa	17% @ 24.0 °C				167 W/m.K	

Table 2 – Chemical composition and physical properties of AA7075-T6.

Materials	Mg	Si	Cu	Cr	Mn	Ti	Zn	Fe	Al
% of composition	2.1–2.9	0.4	1.2–2	0.18–0.28	0.3	0.2	5.1–6.1	0.5	Balance
Physical Property	Melting Point		UTS	Elongation at Break in 50 mm				Thermal Conductivity	
Values	477 °C		572 MPa	11% @ 24.0 °C				130 W/m.K	

Table 3 – Chemical composition and physical properties of AA2011-T3.

Materials	Bi	Si	Cu	Pb	Ti	Zn	Fe	Al
% of composition	0.2–0.6	0.4	5–6	0.2–0.6	0.1	0.3	0.7	Balance
Physical Property	Melting Point		UTS	Elongation at Break in 50 mm			Thermal Conductivity	
Values	540 °C		379 MPa	15% @ 24.0 °C			151 W/m.K	

Table 4 – Chemical composition of AISI 1018 low carbon steel.

Materials	Mn	P	S	C	Fe
% of composition	0.60–0.90	≤0.040	≤0.050	0.14–0.20	98.81–99.26
Physical Property	Melting Point	UTS	Elongation at Break in 50 mm		Thermal Conductivity
Values	1480 °C	440 MPa	15% @ 24.0 °C		51.9 W/mK

Table 5 – Materials and process parameters employed in the experiments.

Sample Number	Type of Material	Tool Rotational Speed (rpm)	Normal Force (N)
1	AA2011	2300	100
2	AA2011	2300	200
3	AA6061	2300	100
4	AA6061	2300	200
5	AA7075	2300	100
6	AA7075	2300	200
7	AA2011	3000	100
8	AA2011	3000	200
9	AA6061	3000	100
10	AA6061	3000	200
11	AA7075	3000	100
12	AA7075	3000	200

full coverage. The developed samples were subjected to SEM and EDS analyses for metallurgical characterization [46]. In another investigation [47], the LFS technique was successfully employed to deposit 6063 aluminum alloy onto A36 mild carbon steel. The experimental result exhibited that the applied force significantly impacted the coverage and surface roughness of the deposited coatings in the LFS technique. Moreover, it was revealed that higher applied tool rotational speed resulted in thicker coating layers. In [48], the corrosion performance of AA1100, AA2024, AA5086, AA6061, and AA7075 coatings deposited onto AISI 1018 was evaluated by mass loss measurement through an accelerated corrosion test, and it was revealed that AA5086 provided the most protection. There is not much literature on LFS as this is a relatively new friction stir processing technique.

Despite these findings obtained from previous studies, the effect of different alloys composition on the mechanical and metallurgical properties of the coating has not been studied. The hypothesis is that aluminum alloys will perform differently in LFS in accordance with their material properties, and that the mechanical properties will be more important for this relatively low temperature LFS process. Three aluminum alloys with different strength and thermal properties were chosen to investigate this hypothesis. The effect of process factors and alloys composition on processing behaviors, physical properties, and metallurgical characteristics of the depositions are fully quantified for three different aluminum

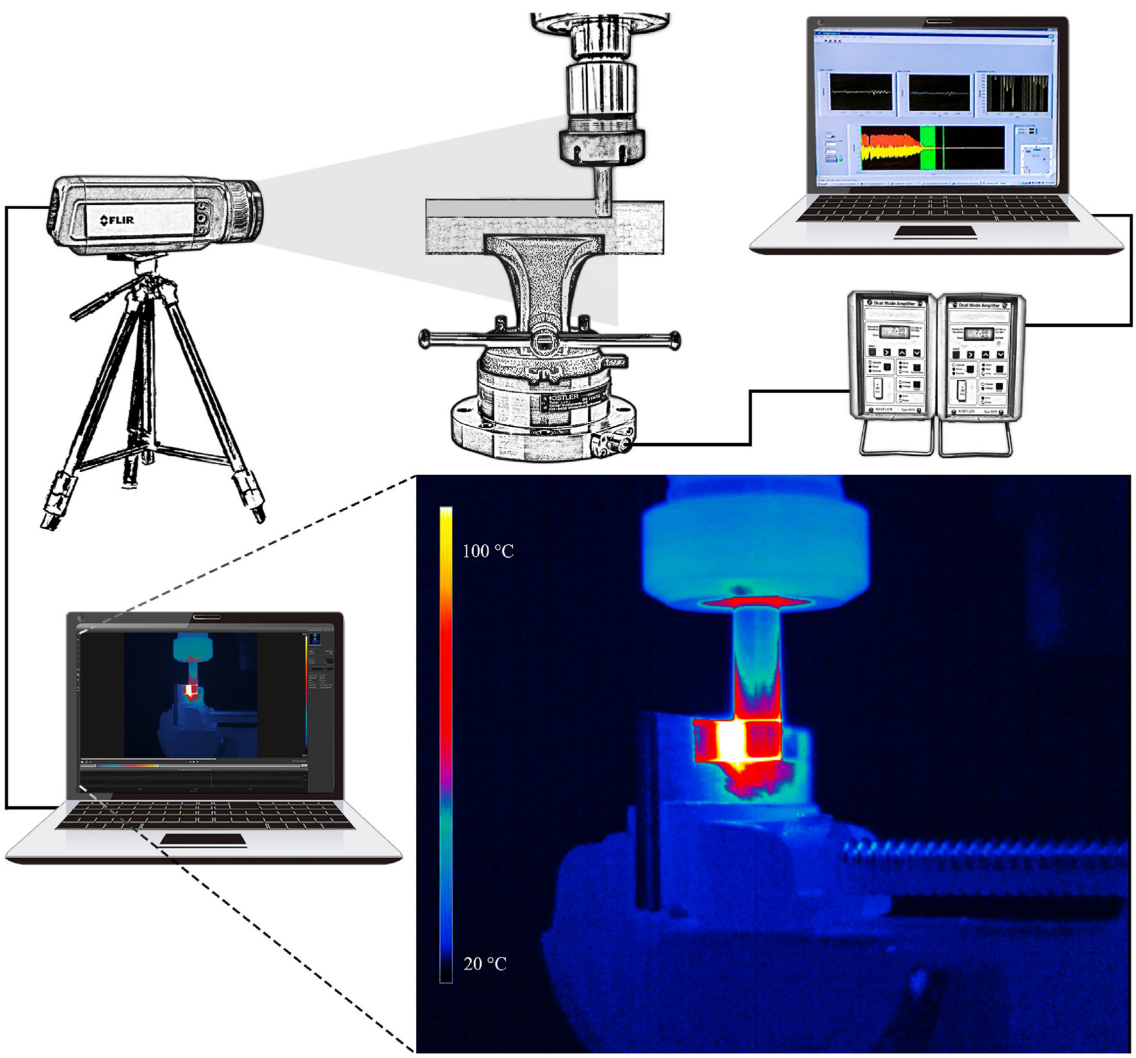

Fig. 2 – Demonstration of experimental setup utilized in LFS approach.

alloys, AA2011, AA6061, and AA7075 onto AISI 1018 carbon steel. Critical process variables such as spindle speed and applied load have been considered as the process controlling parameters. This novel method of LFS gives a possibility of creating ultra-thin and smooth deposited coating developed in lower temperatures compared to many joining methods as well as the conventional FS technique, which reduces thermal impacts on metallurgical properties and grain structures of the coatings. The focus of the present investigation is the understanding of the correlation between process parameters and the resulting coating and tool properties, i.e., surface roughness, coating thickness, coating coverage, material deposition rate, microstructures, as well as the process temperature.

2. Materials and methods

In this investigation, the novel approach of LFS was utilized to fabricate the friction deposits of three different types of aluminum alloys, AA2011, AA6061, and AA7075, onto an AISI 1018 carbon steel substrate. The radial surface of the consumable rod was forced against the substrate surface, and material transfer occurred from the side of the tool. Plasticization of the consumable material was caused by frictional heat generated between the rotating consumable tool and the substrate. This research is an attempt to understand the basic principles of the LFS process with a special attention to the impacts of process parameters and different consumable materials on the deposited coatings. In the LFS, the radial surface of the consumable tool in contact with the surface of the substrate experiences a constant rotational velocity at the interface, which results in a consistent deposition compared to the conventional FS technique. This also means unlike the conventional approach, there is no retreating and advancing side in the LFS approach.

2.1. *Materials and experimental parameters*

The purpose of this study was to quantify the effect of different material properties on the process and coating quality in LFS. Three different types of aluminum alloys, AA2011, AA6061, and

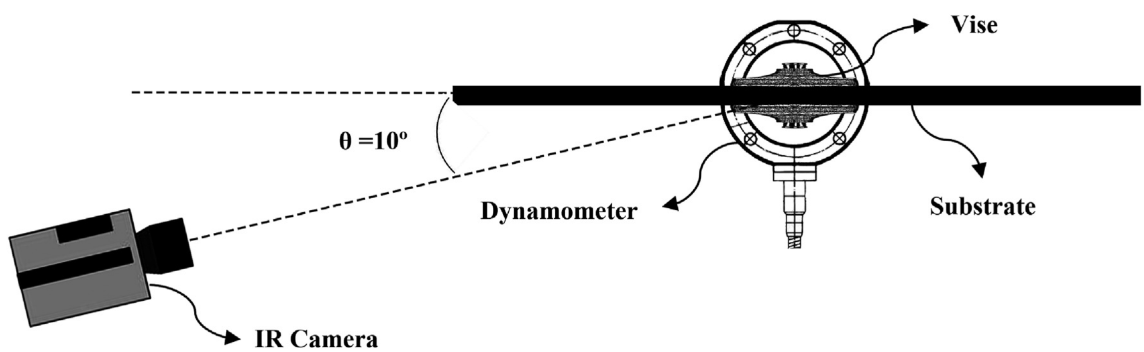

Fig. 3 – Configuration of IR thermography setup during the LFS process from top view.

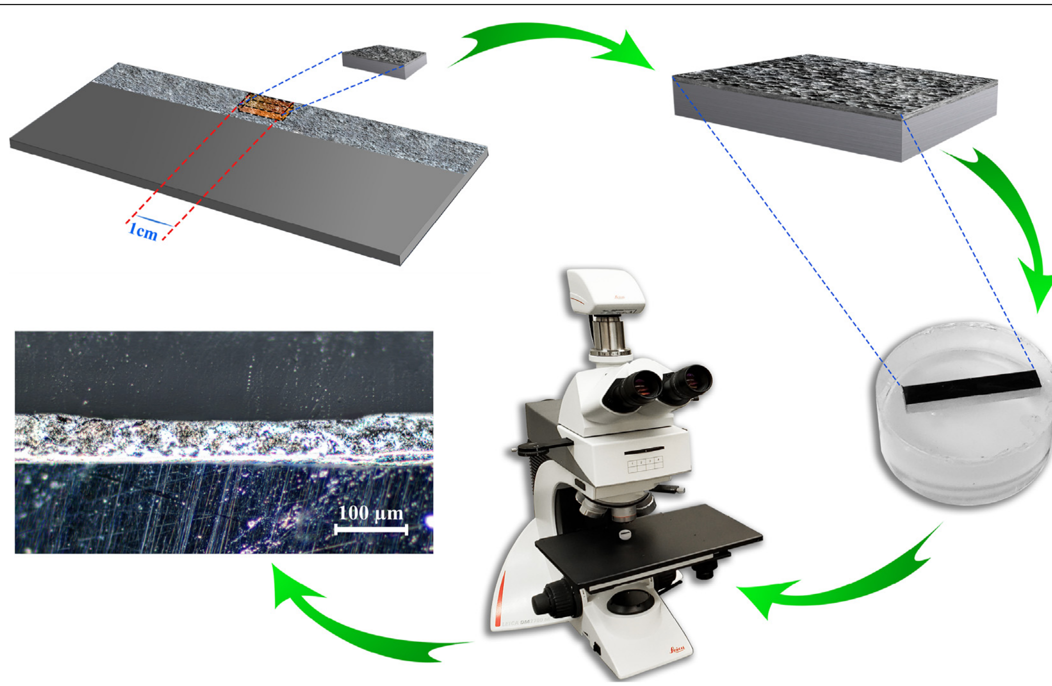

Fig. 4 – Cross-sectioning of the deposited coatings.

AA7075, were utilized as the consumable rods with a length of 10 cm and a diameter of 1.27 cm. The chemical composition and some physical properties of consumable materials are presented in Tables 1–3 [49]. These three kinds of aluminum alloys are different in terms of structure, composition, and material properties. AA6061 is the most common alloy used in friction stir processing due to high formability, workability, and weldability. As shown in Table 1, it has silicon and magnesium as the major alloying elements and has the highest ductility, melting point, and thermal conductivity, but has the lowest strength. On the

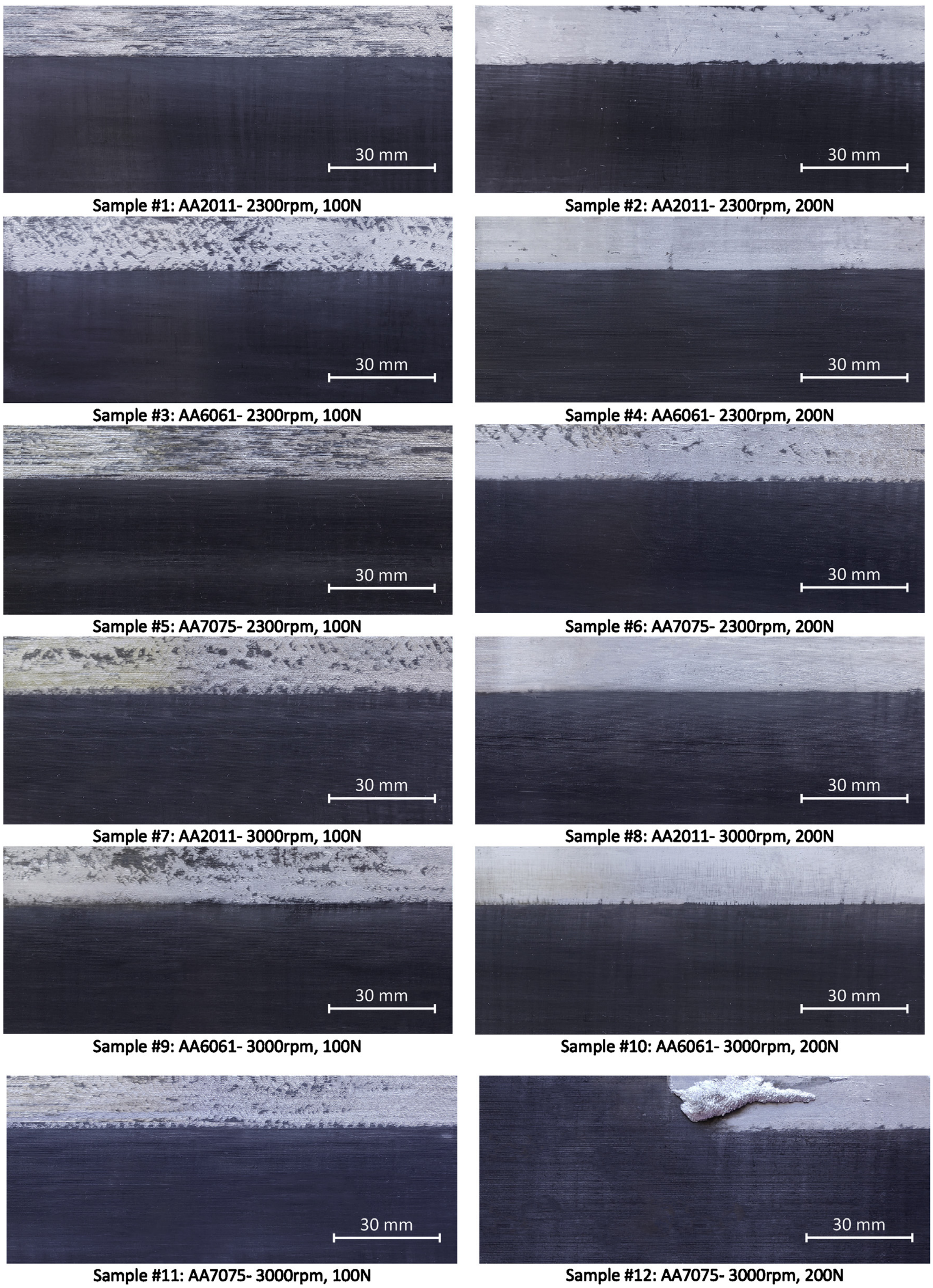

Fig. 5 – Experimental samples developed by LFS using different process parameters.

other hand, AA7075 with zinc as its primary alloying element is an exceptionally high strength aluminum alloy, comparable to many types of steel. Although this alloy presents a high tensile strength, it has lower melting temperature, thermal conductivity, and ductility. AA2011 has a higher percentage of copper as its principal alloying element resulting in high toughness and strength. The thermal and strength properties presented in Table 3 have values in between those of AA6061 and AA7075.

The tool substrate material was AISI 1018 with a thickness of 3.18 mm and the dimensions of 127 mm × 50.8 mm. This material was selected since it also has a wide range of industrial applications due to its great performance in various processes such as heat treating, welding, forging, and machining. The chemical composition, as well as some physical properties of AISI 1018, are presented in Table 4 [49].

Two different spindle speeds of 2300 and 3000 rpm, and two different applied forces of 100 and 200 N were experimented. A constant traverse speed of 76.2 mm/min was considered as the longitudinal movement of the table. The applied force on the side of the consumable tool keeps the rod in continuous contact with the substrate; and the normal force was held constant as the workpiece moved laterally; therefore, there was no gap between the rod and substrate. Table 5 presents the details of material and process parameters employed in each sample in this study. These values were chosen based on the previous experimental experiences obtained from the LFS of different materials, as well as the capability of the machine and measuring equipment. It has been determined from a first-principles study that LFS with a low force results in insufficient coating coverage and thickness. Also, LFS with high force results in material breakdown in the tool due to high plastic deformation and load bearing limitations.

2.2. *Experimental setup and measurement procedure*

The LFS process was conducted by employing a customized JET JMD-18 milling machine. In order to increase the accuracy of the experimental study and provide a consistent and controlled longitudinal movement by the machine, the manual feed handle installed on the table was detached, and the table of the milling machine was equipped with a servo power feed controller. In other to control the applied force and record the normal and tangential forces during the process, a four-component Kistler drilling dynamometer type 9272, data acquisition systems, and LabVIEW programming were utilized, as shown in Fig. 2. Moreover, the original chuck arbor of the JET JMD-18 milling machine was replaced by an ER40 collet chuck tool holder to provide better maneuverability with shifting between different sizes and types of tools.

Infrared (IR) thermography was performed using an IR FLIR SC655 camera to record the process temperature during the LFS. Infrared thermography is a non-contact and convenient approach to provide a real-time temperature measurement during the process. The IR camera records the process temperature based on the irradiance from the surface of an object. The IR camera employed in this study was calibrated to measure process temperatures between 0 and 650 °C. LFS can be done at temperatures less than consumable material's (aluminums) melting points, which is perfectly fitted in the measuring range of the IR camera. The camera was located at an appropriate distance of 0.5 m from the processing area in a way that the focus was made on the surfacing zone at the interface at an angle of 10° with the substrate, as shown in Fig. 3. The consumable tools and substrates were cleaned by ethanol prior to the deposition process to remove grease and powder. Then, the surface of the substrate was covered by a thin graphite layer which increases the surface emissivity up to 0.80 [50]. The aim of this measurement is to investigate the influence of the generated heat at the interface of the substrate and rotating tool on the process behavior and coating properties.

The surface roughness analysis is one of the most important surface examinations in evaluating the superficial properties of coatings. Surface roughness has a significant impact on various important physical phenomena such as friction, sealing, adhesion, and wear behavior. In the present study,

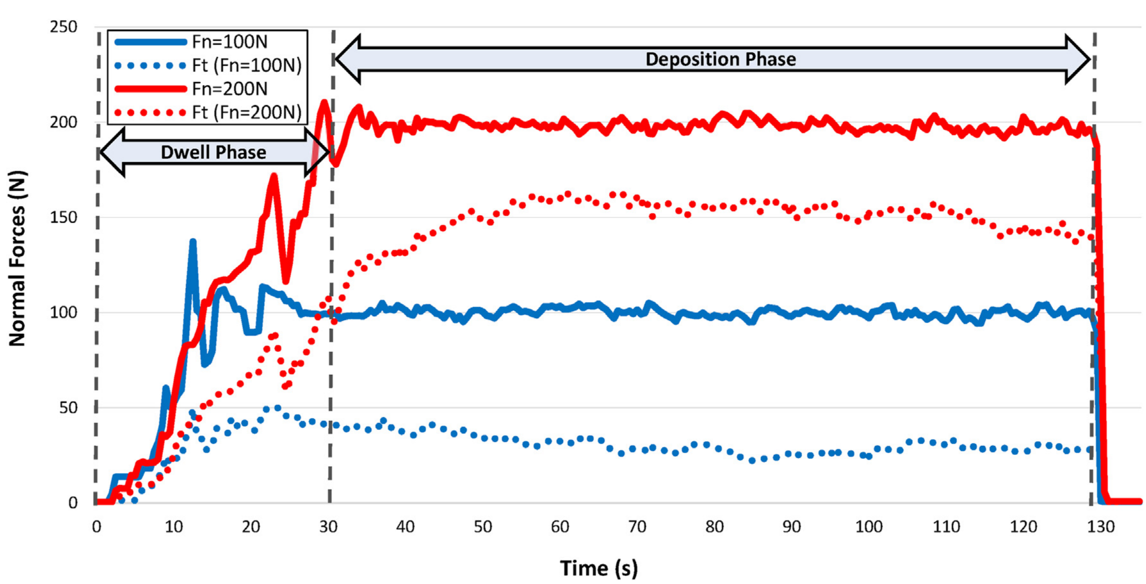

Fig. 6 – Normal and tangential forces during LFS of sample 1 (blue) and sample 2 (red).

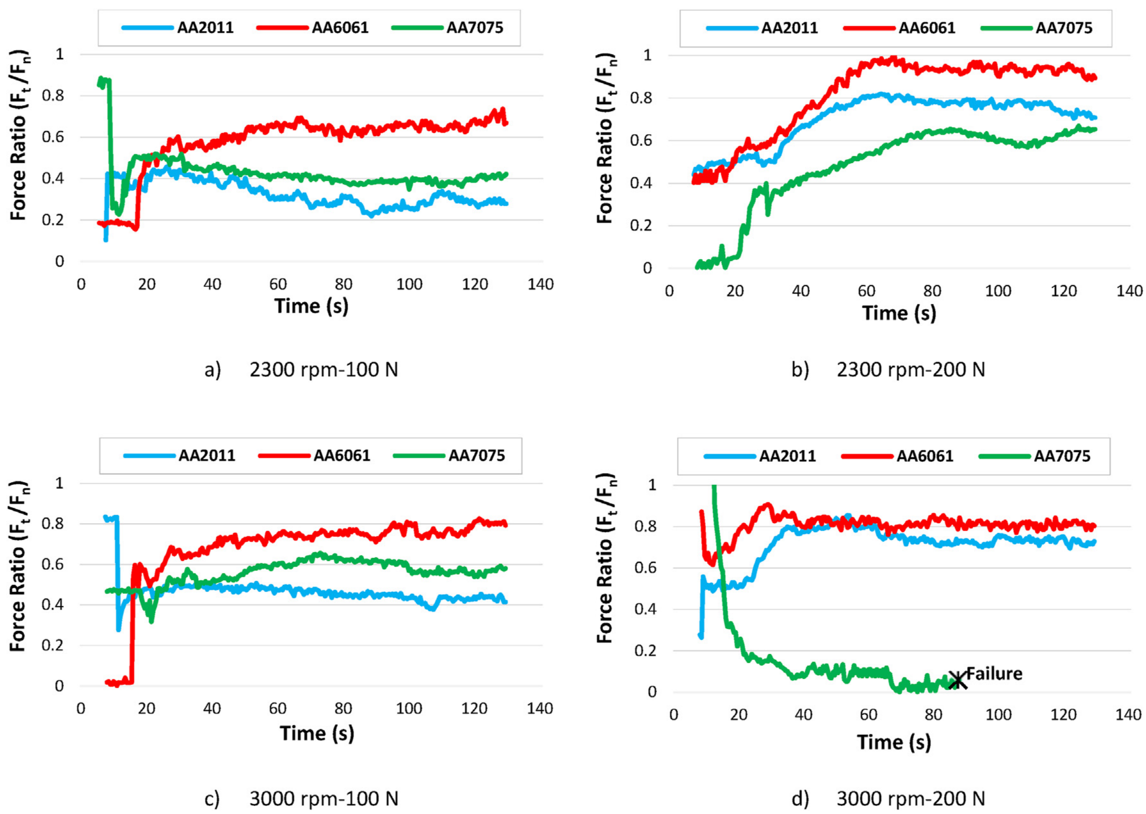

Fig. 7 – Force ratio during the LFS process.

the influence of the process parameters such as spindle speed, applied force, and type of consumable material on the surface roughness of the developed deposits is evaluated. The roughness of the deposited coatings was characterized utilizing Ra, the arithmetic means deviation of the coating surface profile. For this purpose, a Landtek SRT6200S surface roughness tester with the great resolution of 0.001 μm in measuring surface roughness values less than 10 μm, was employed to evaluate the surface roughness values of deposited coatings as well as the substrate without coating, as

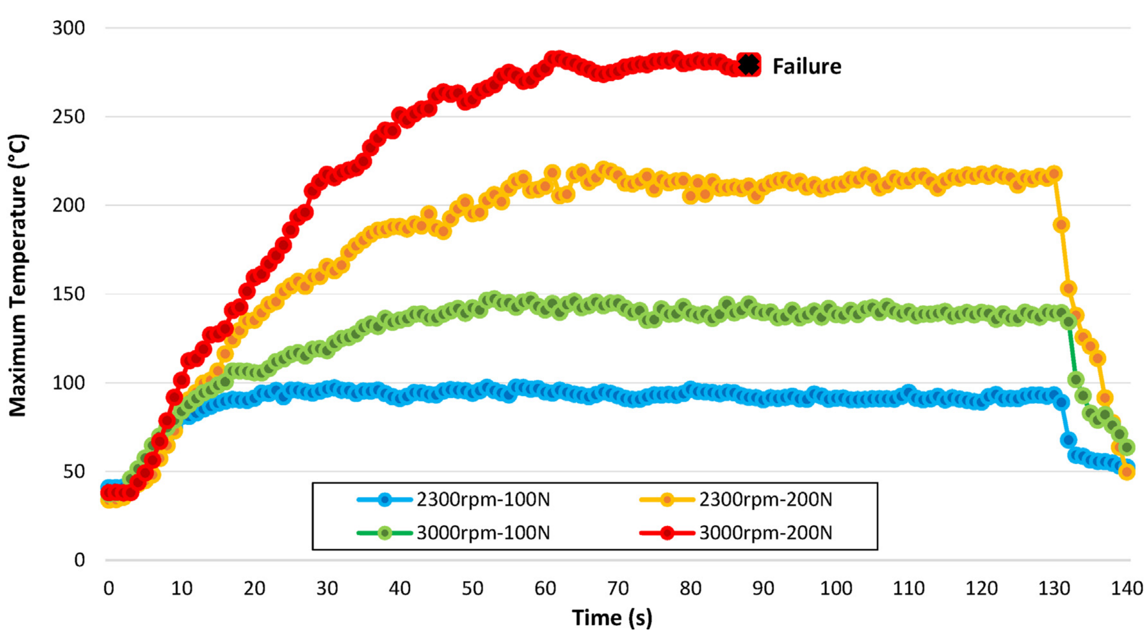

Fig. 8 – Evolution of maximum process temperature during LFS of AA7075.

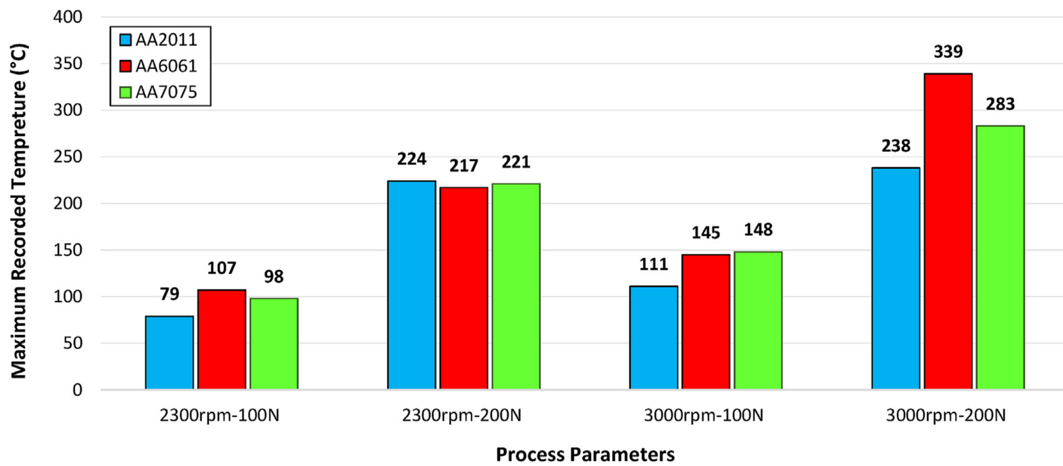

Fig. 9 – Maximum recorded temperature during the LFS process.

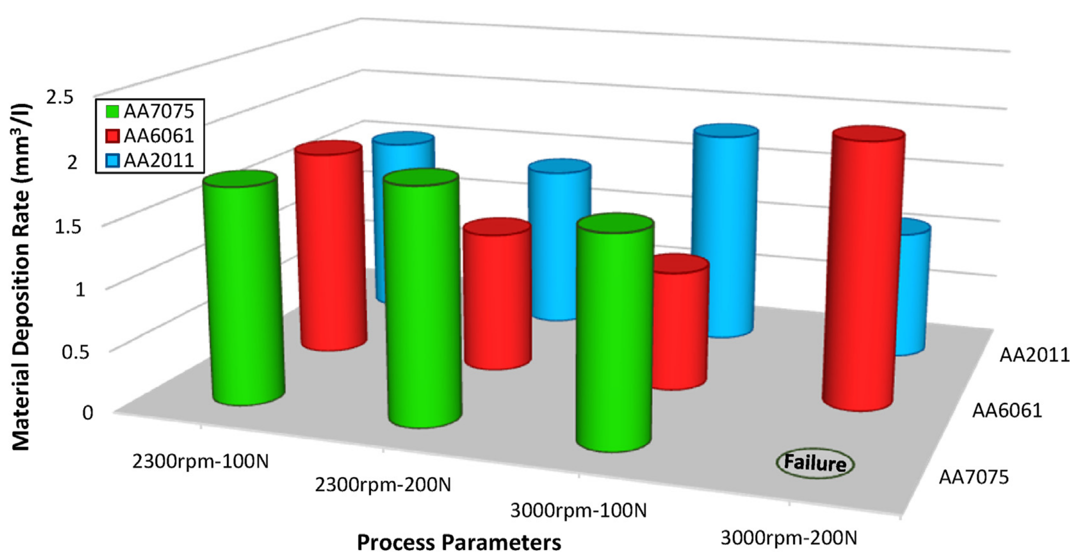

Fig. 10 – Tool material deposition rate during LFS process.

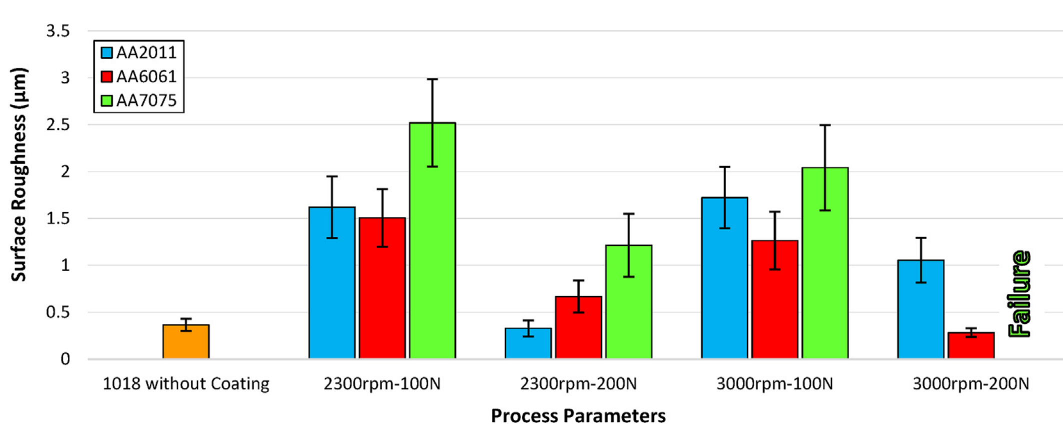

Fig. 11 – Surface roughness during LFS process.

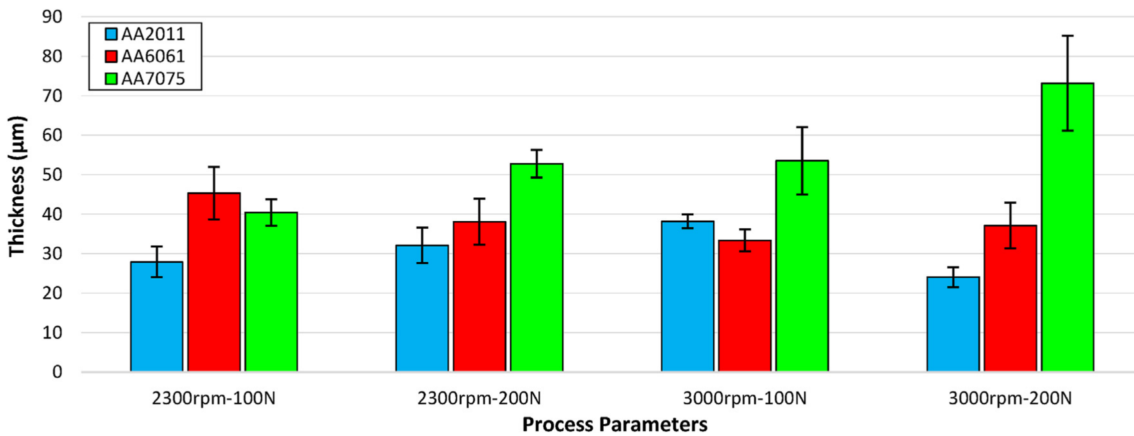

Fig. 12 – The average thickness of fabricated layers created by different sets of process parameters.

received. The material deposition rate was evaluated by measuring the reduced volume of the consumable tools during the LFS process.

2.3. *Microscopy*

The cross-sectional viewing of the coating layers and the influence of process parameters on their thickness values are investigated by means of a Leica optical microscope type DM2700. For this purpose, 1 cm of the deposited coatings was cut to be mounted in epoxy, as shown in Fig. 4. Then, the samples were polished by utilizing 1 μm and 0.3 μm aluminum oxide abrasive particles, prior to cross-section viewing using optical microscope.

The interface and the deposits fabricated through LFS were investigated using Scanning Electron Microscopy (SEM).

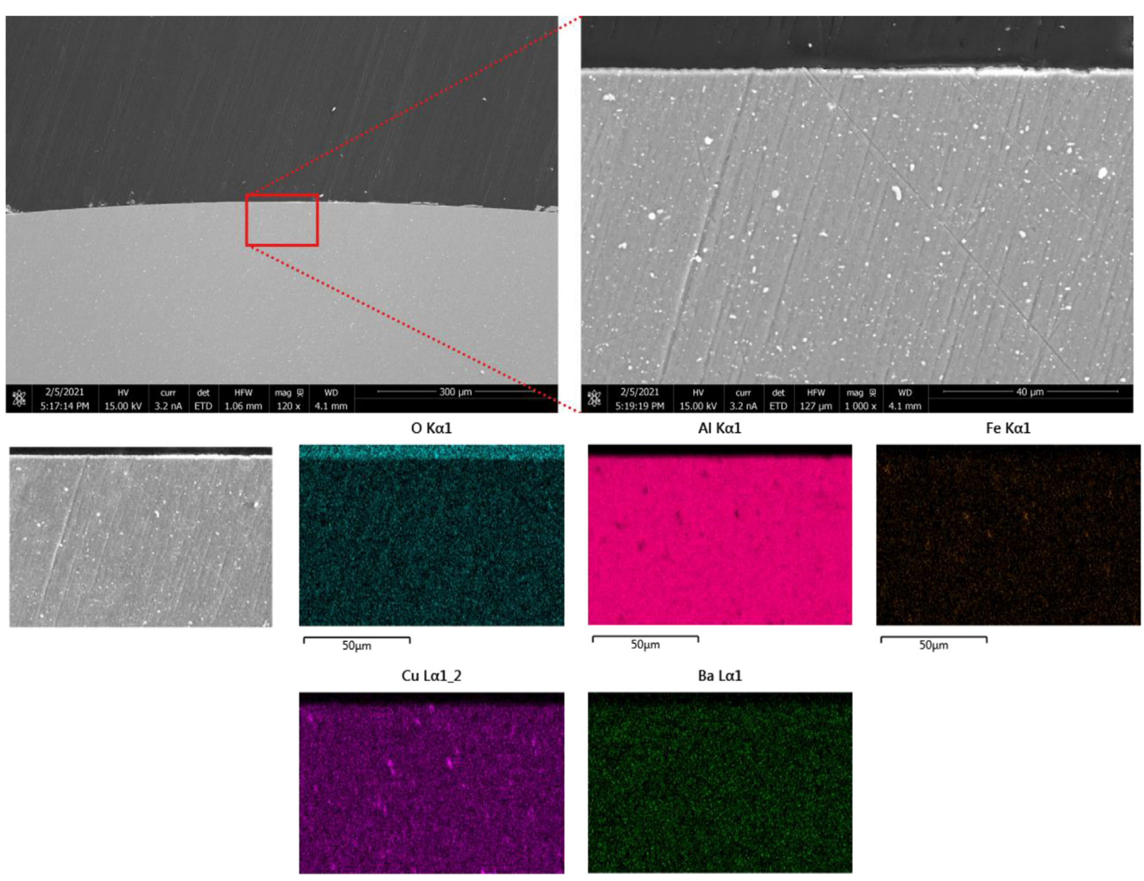

Fig. 13 – SEM images and EDS maps of the consumable rod material AA2011.

Cross-sectional characterization of different deposited materials using SEM provides further information regarding the interfaces and the impacts of process parameters and type of materials on the development of cracks and bonding quality between the coating and substrate. Moreover, EDS analysis was conducted to identify the composition of the deposited material and the participated elements. For this purpose, a FEI Helios NanoLab 660 Dual-Beam SEM-FIB equipped with an Oxford Instruments X-Max EDS system was employed.

3. Results and discussion

In this study, an ultra-thin coating layer of AA2011, AA6061, and AA7075 aluminum alloys were fabricated onto the surface of AISI 1018 carbon steel by LFS approach. The visual assessment of deposited coating layers presented in Fig. 5 shows that process parameters significantly influenced the coating coverage and roughness. It was observed that higher normal force resulted in more significant deposition. As is shown in sample 12, the deposition of AA7075 using high tool rotational speed and normal force failed due to high input energy, which possibly resulted in an unstable condition of severe plastic deformation and shearing of the consumable material. During the process, a large amount of softened material was suddenly deposited on the substrate, resulting in the failure of the LFS process. This indicates that there are limitations in using the very high or low values of process parameters in deposition of different consumable materials.

3.1. *Measured forces and temperature during the process*

Figure 6 shows the measured normal and lateral forces during LFS. The normal force was manually controlled at 100 and 200 N shown by the solid lines after a 30 s dwell period to bring the force and temperature to steady state. At the 30 s mark, the horizontal feed of the table was started at 76.2 mm/min. The dotted lines show the lower tangential forces correlating to 100 and 200 N normal force. A real-time force ratio for each material and set of process parameters was recorded by measuring the normal force (F_n) and the tangential force (F_t) at any moment during the process, as shown in Fig. 7.

The normal forces employed in this technique were much lower compared to that in several investigations on the conventional FS process [7,9,11], while it can deposit coatings with good coverage and reduce the risk of damage to the machine, equipment, and tool. The result of the force measurement revealed that the tangential force was lower than the normal force for all the materials, as shown in Fig. 7. Moreover, the force ratio (F_t/F_n) was the highest for AA6061 for all employed parameters, exhibiting a higher friction coefficient for this alloy during the process. This was also

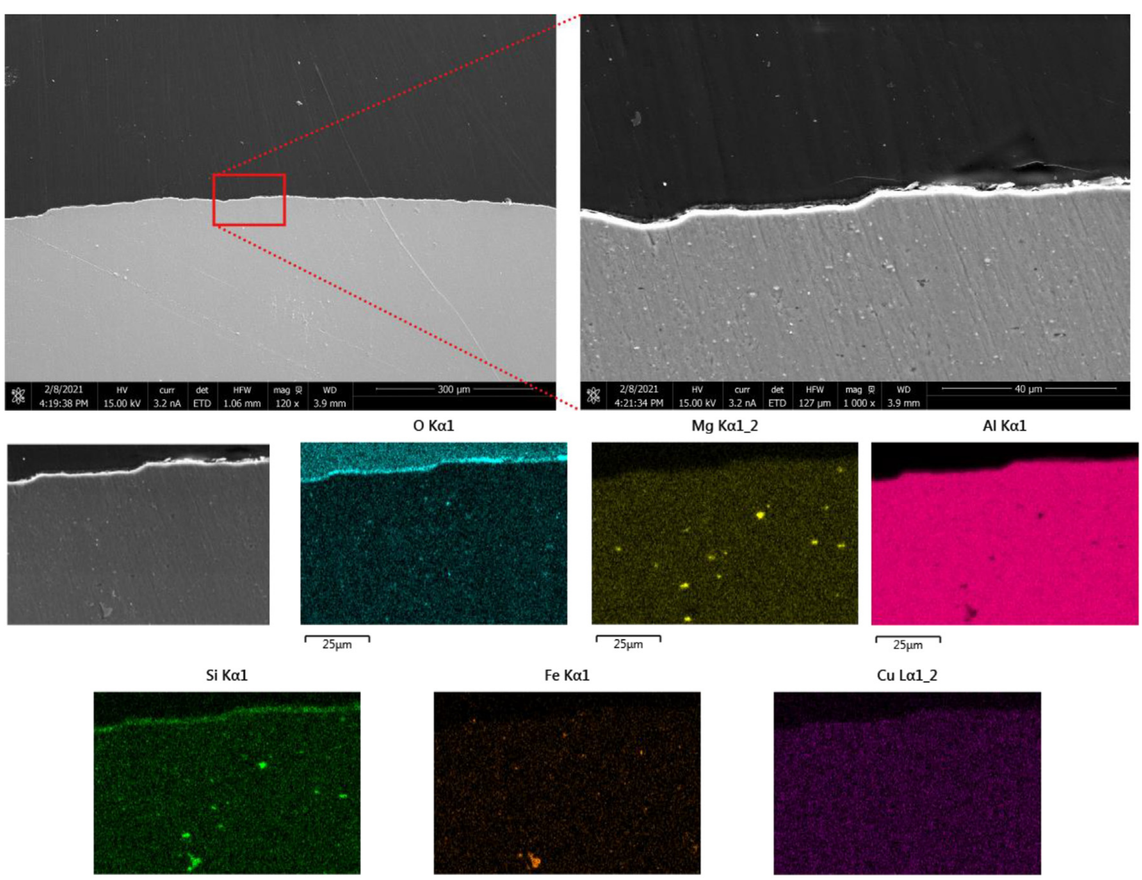

Fig. 14 – SEM images and EDS maps of the consumable rod material AA6061.

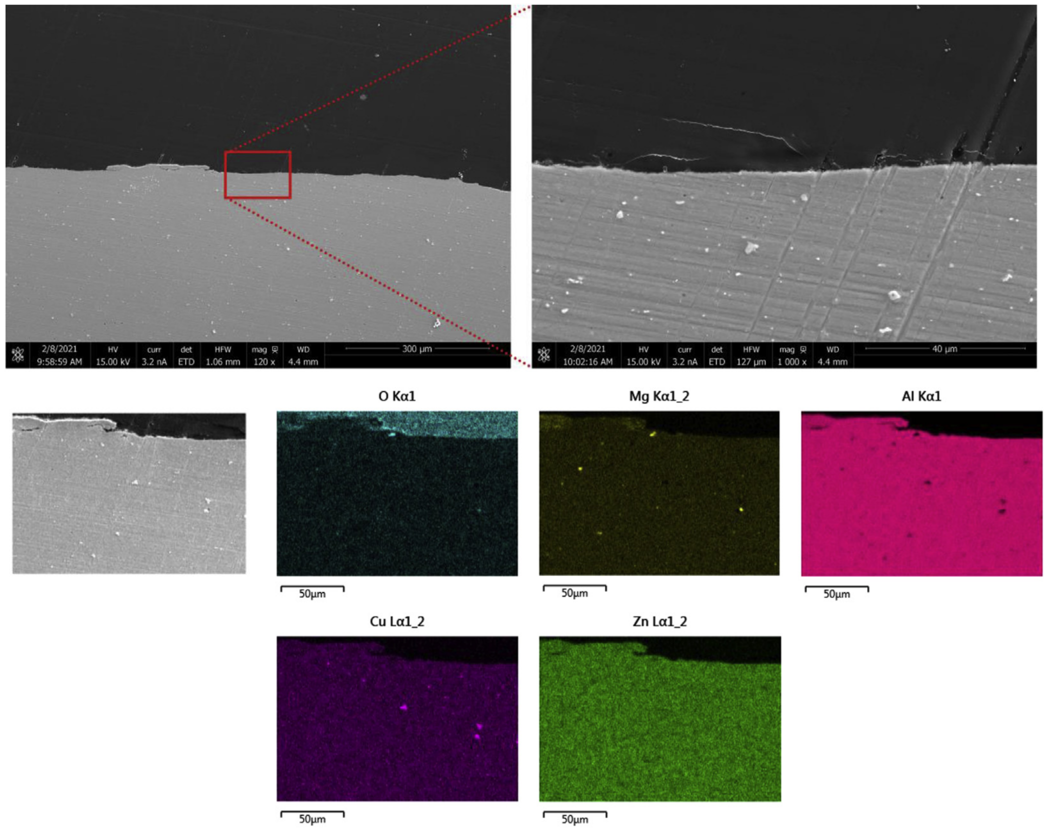

Fig. 15 – SEM images and EDS maps of the consumable rod material AA7075.

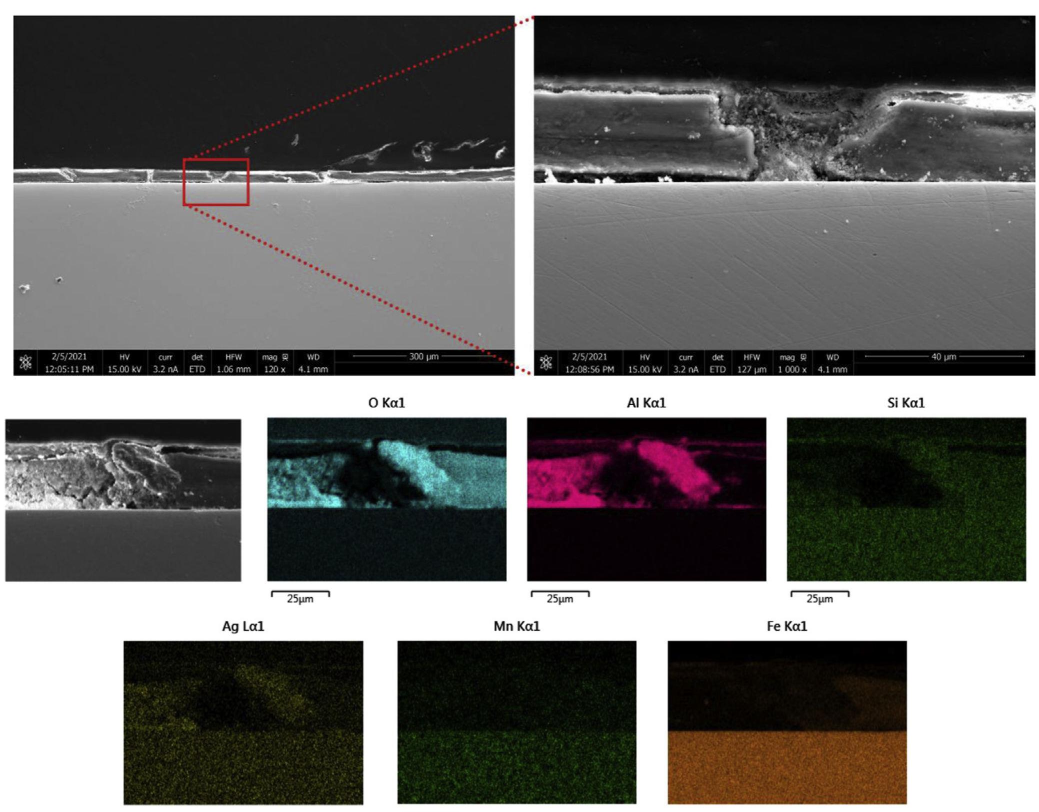

Fig. 16 – SEM images and EDS maps of the AA2011 deposit fabricated by 2300 rpm and 200 N.

previously confirmed that AA6061 has a higher friction coefficient than several aluminum alloys, such as AA7075 [51]. In most of the experiments, the force ratio experiences a steady state after a small increment. This shows that the friction coefficient increases as the temperature rises, and it reaches to a steady state as the process temperature reaches a steady state. Also, Fig. 7(d) shows that the friction coefficient for AA7075 decreases as this material softened due to high temperature and then decreased to zero before the failure point. This phenomenon is entirely compatible with the principle that softened materials at high temperatures have lower shear strength.

Infrared (IR) thermography was performed using an IR FLIR SC655 camera to record the process temperature during the LFS process. The presented results in Fig. 8 illustrate how the process temperature changes depending on the tool rotational speed and normal force employed in the process. The process temperature can be raised either by higher energy input developed due to employing an increased normal force or tool rotational speed, or due to a lower thermal conductivity of the tool/substrate materials. The AA7075 consumable material utilized in this study has a lower thermal conductivity and melting point compared to AA2011 and AA6061, which creates limitations in using high values of normal forces and tool rotational speeds. As is shown in Fig. 8, the LFS of AA7075 using tool rotational speed of 3000 rpm and normal force of 200 N failed due to high input energy, which resulted in severe plastic deformation and softened consumable material.

For the different consumable materials investigated in this study, the maximum difference in process temperature developed by low values of process parameters of 2300 rpm and 100 N was 28 °C, while for high values of 3000 rpm and 200 N was 101 °C. The maximum recorded temperatures during each experiment are presented in Fig. 9. The result exhibited that increasing the spindle speed and normal force result in a higher maximum process temperature. Furthermore, it was revealed that the normal force has a more significant impact on the process temperature than the tool rotational speed. Therefore, it can be concluded that the thermal properties of the consumable materials and both employed process variables significantly affect the process temperatures, which determine the resulting deposit's geometry and metallurgical properties. The lowest process temperature in this study was as low as 79 °C developed in LFS of AA2011 using tool rotational speeds of 2300 rpm and normal force of 100 N, and the highest process temperature was 339 °C developed in LFS of AA6061 using tool rotational speeds of 3000 rpm and normal force of 200 N. The process temperature generated in this technique is significantly lower than that in the conventional FS of aluminum alloys. The process temperature in the FS of AA7075 onto AA5754 using traverse speed of 120 mm/min and vertical feed rate of 160 mm/min was reported as 459 °C and 496 °C for tool rotational speeds of 1000 and 1200 rpm, respectively [52]. In another investigation, FS of AA7075 consumable tool onto AA5754 substrate generated the maximum temperature of 547 °C using traverse speed of

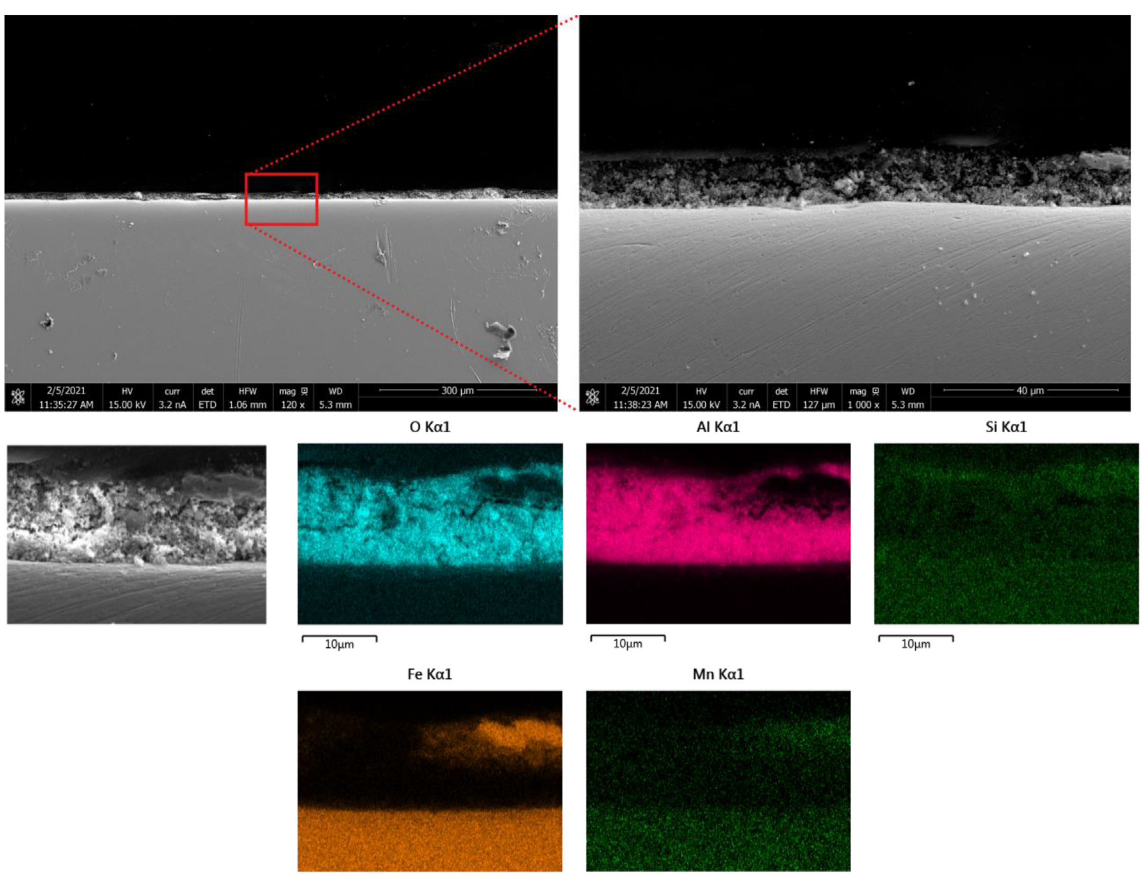

Fig. 17 – SEM images and EDS maps of the AA2011 deposit fabricated by 3000 rpm and 200 N.

160 mm/min, vertical feed rate of 100 mm/min and tool rotational speed of 1000 rpm [53].

3.2. Influence of process parameters on deposition

There is no flash formation in the LFS process, which is advantageous for this approach compared to the conventional FS technique. It was exhibited that flash formation is a critical issue that can waste up to 60% of the tool consumable material [54]. In this study, the material deposition rate was measured by determining the reduced volume of rod consumable material during the process. Generally, the higher values of material deposition rate during the LFS process and a lower coverage result in thicker deposits.

As is presented in Fig. 10, there is no particular trend in the material consumption rates of the different types of aluminum with respect to the process parameters, which exhibits the complexity of process parameters' impacts on the resulting deposits. The highest rates of material deposition rates through successful LFS processes for AA2011, AA6061, and AA7075 were observed at 3000 rpm and 100 N, 3000 rpm and 200 N, 2300 rpm and 200 N, respectively. The material deposition rate of AA7075 using different process parameters is noticeable, which indicates that a larger amount of AA7075 consumable material can be plasticized and sheared through LFS. This makes sense due to the lower thermal conductivity, melting point, and ductility of this alloy which increase accumulation of heat at the processing area resulting in a severe plasticization of the consumable material.

In order to investigate the effect of the different process parameters and types of consumable materials on the roughness of the coated deposits, the deposited samples, as well as the substrate without coating, were subjected to surface roughness evaluation. For this purpose, 20 different random points on the samples' surfaces were selected and tested, and the average surface roughness values of selected spots were recorded as presented in Fig. 11. The presented error bars present the standard deviations from the means.

As is shown in Fig. 11., aluminum coating layers with the surface roughness values in the order of about 1–2 μm were produced. Fabricating a layer of the aluminum alloys onto the surface of 1018 steel substrate generally increases the surface roughness; however, it would be even smoother in few cases. It is also shown that LFS of the more brittle AA7075 resulted in the roughest deposited coatings compared to the other two consumable aluminum alloys. It is hypothesized that high temperature shear strength was compromised in AA7075, which has lower melting point and thermal conductivity. Furthermore, it is exhibited that applying higher normal force results in smoother surfaces. The roughness of the smoothest deposit was as low as 0.28 μm developed through LFS of AA6061 using tool rotational speeds of 3000 rpm and normal force of 200 N. The roughness of the roughest deposit was 2.5 μm, which was developed through

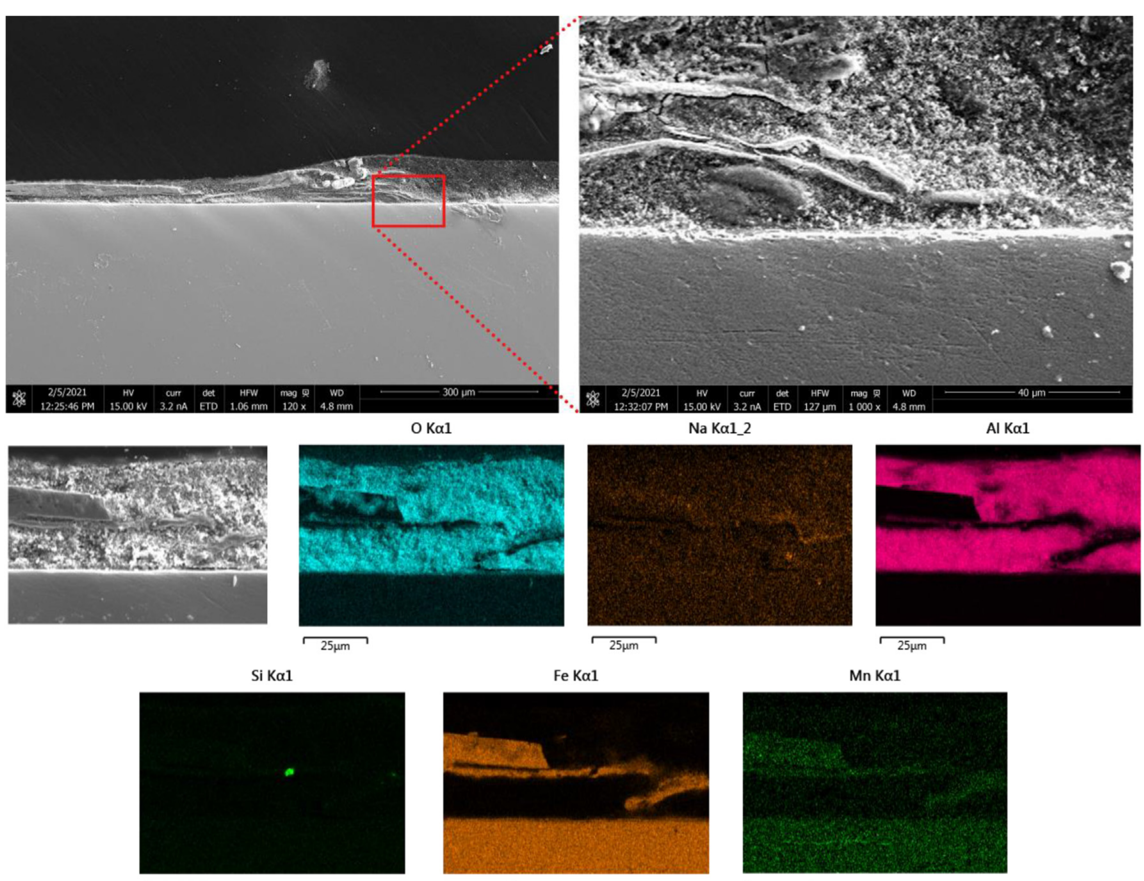

Fig. 18 – SEM images and EDS maps of the AA6061 deposit fabricated by 2300 rpm and 200 N.

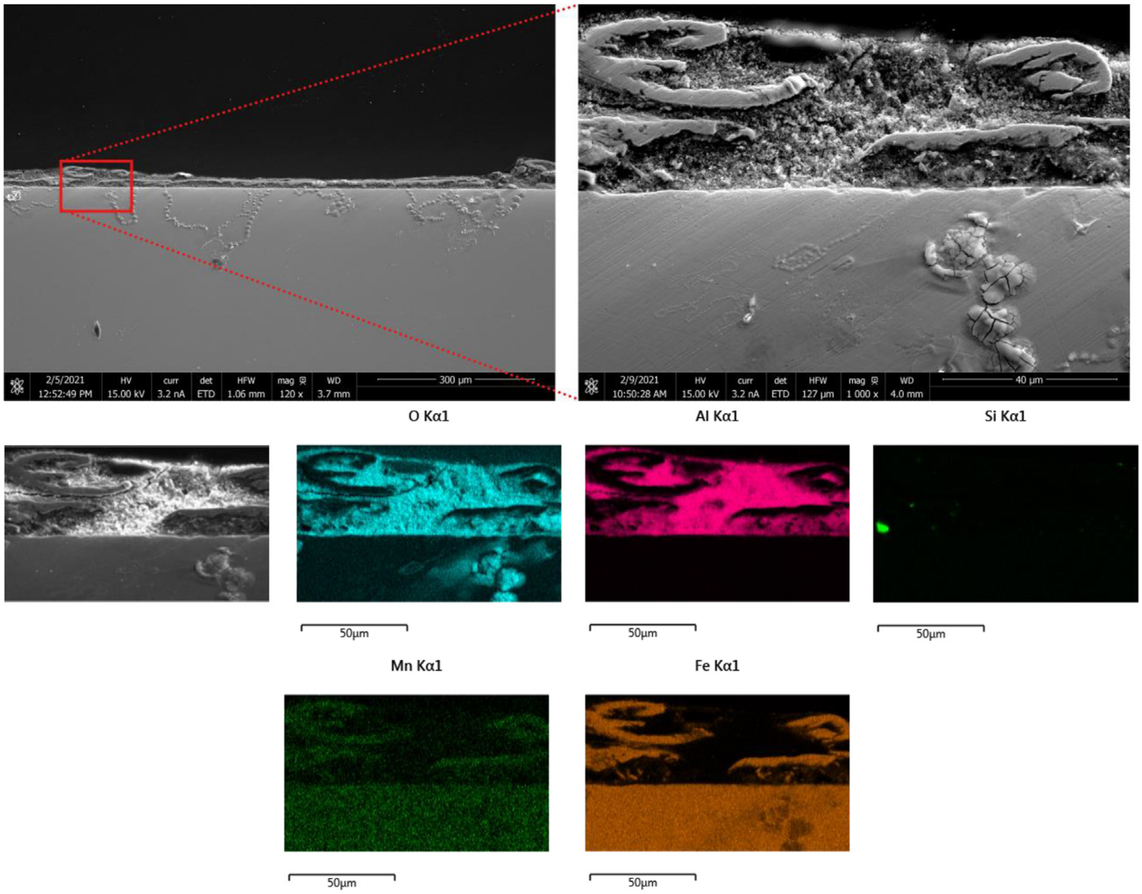

Fig. 19 – SEM images and EDS maps of the AA6061 deposit fabricated by 3000 rpm and 200 N.

LFS of AA7075 using tool rotational speeds of 2300 rpm and normal force of 100 N.

The cross-sectional viewing of the deposited layers was conducted using a Leica optical microscope type DM2700 at the magnification of 20×. The highest thickness value was observed in before failure in LFS process of AA7075 by employing 3000 rpm and 200 N, while these process parameters resulted in the lowest coating thickness value in LFS

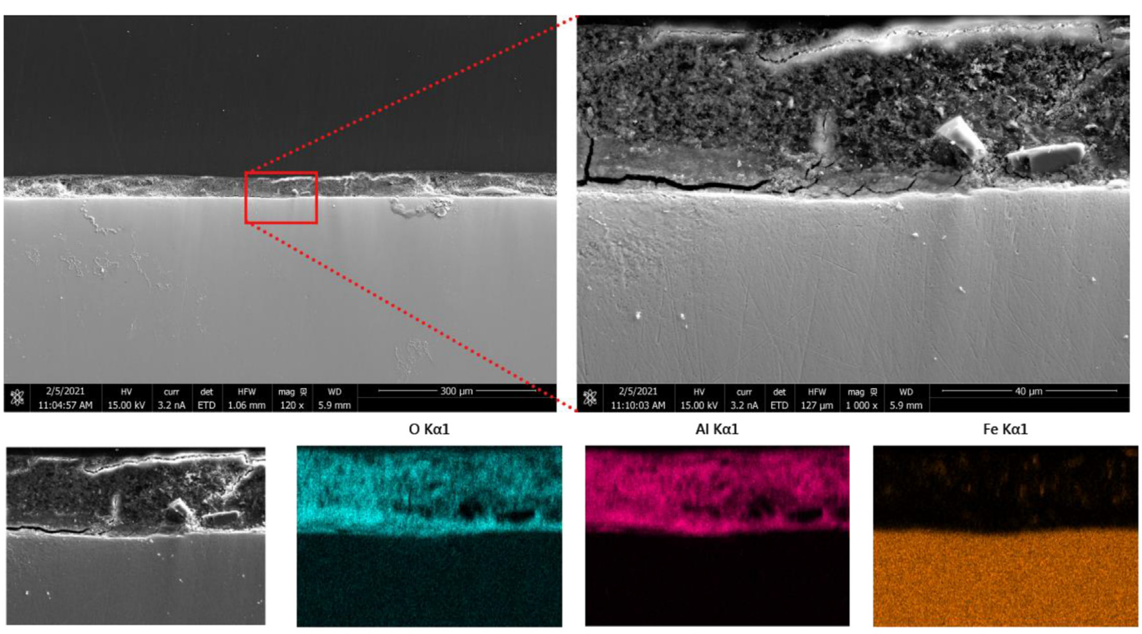

Fig. 20 – SEM images and EDS maps of the AA7075 deposit fabricated by 2300 rpm and 200 N.

process of AA2011. The lowest and highest average coating thickness values recorded during this process were 24 μm and 73 μm, as presented in Fig. 12. In majority of cases, AA2011 provides the thinnest coating layers, while AA7075 results in thickest deposit layers using different combinations of process factor.

3.3. Material characterization

This study exhibits that LFS is a promising technique for solid-state dissimilar aluminum deposits; however, different materials and process parameters lead to different deposit microstructures, composition, bonding, and coating quality. The quality and composition of the coating is unknown for this new process. The effect of the LFS process on the deposition was qualified on cross-sectioned samples through SEM and EDS analyses. The SEM analysis revealed more information regarding the interfaces and the impacts of process parameters on the cracks, bonding quality, and intermixing between the consumable material and substrate. The EDS analysis was performed to identify the composition of the coatings and the participated elements.

The result of SEM and EDS analysis of as-received aluminum rods are presented in Figs. 13–15. It is important to evaluate the as-received materials to understand if there are any defects or areas with a high amount of a specific element in the consumable material, as it helps to figure out the origin of such possible defects or regions in the deposits. The SEM analysis of the aluminum rods confirms the absence of surface defects and further exhibits that the radial surface of the consumable rods is not completely smooth. The EDS maps of the as-received materials revealed the distribution of various elements in the employed materials before the surfacing process. The result of EDS analysis confirms a uniform distribution for the majority of elements; however, the maps show brighter regions containing high amounts of Cu in AA2011, high amounts of Mg, Fe, and Si in AA6061, and high amounts of Mg and Cu in AA7075.

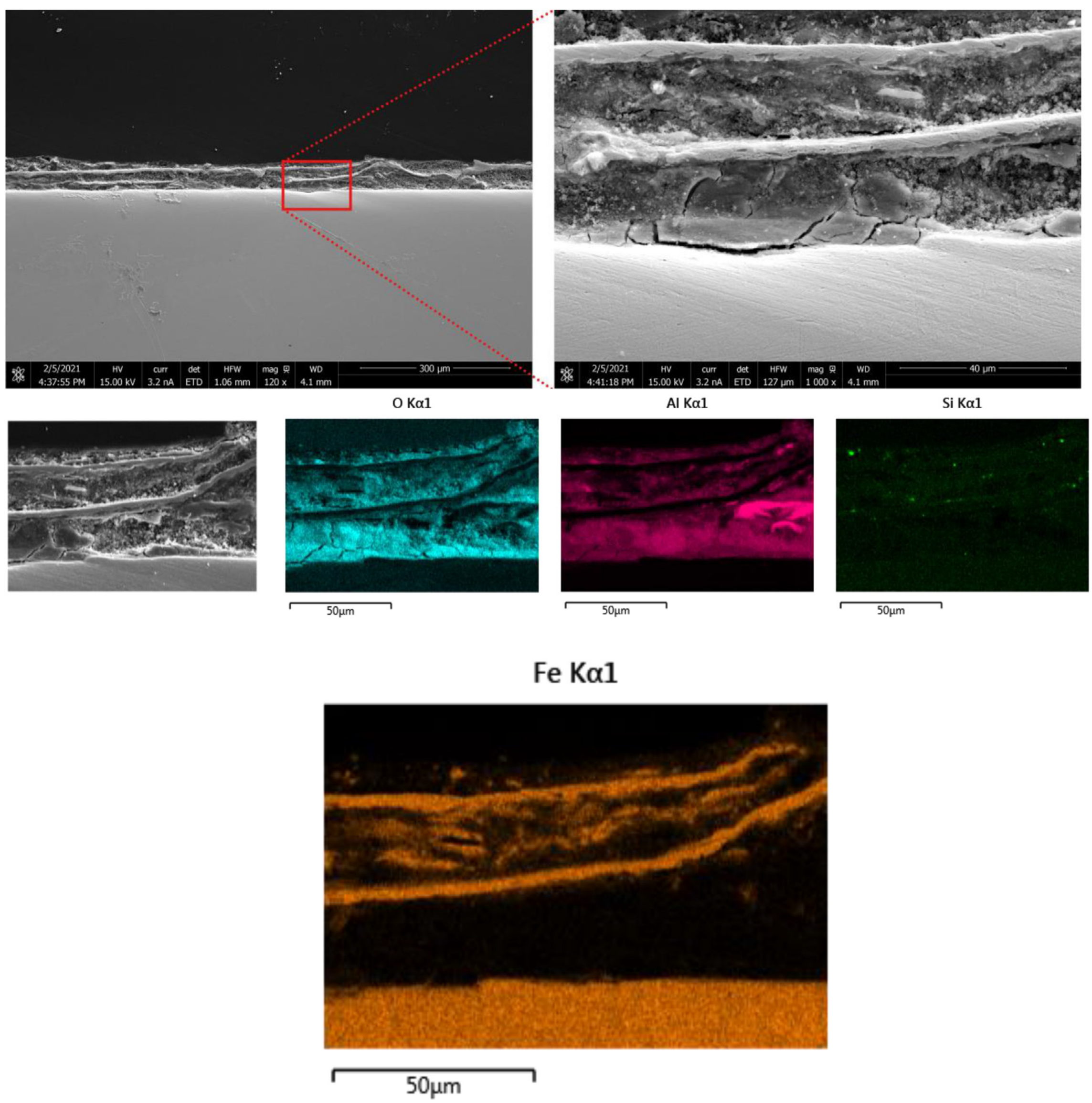

Fig. 21 – SEM images and EDS maps of the AA7075 deposit fabricated by 3000 rpm and 200 N.

Table 6 – Summary of evaluations and analyses.

	Process Parameters	AA2011	AA6061	AA7075
Coverage	2300 rpm, 100 N	I	II	III
	2300 rpm, 200 N	II	I	III
	3000 rpm, 100 N	II	III	I
	3000 rpm, 200 N	II	I	Failure
Force Ratio	2300 rpm, 100 N	III	I	II
	2300 rpm, 200 N	II	I	III
	3000 rpm, 100 N	III	I	II
	3000 rpm, 200 N	II	I	III
Temperature	2300 rpm, 100 N	III	I	II
	2300 rpm, 200 N	I	III	II
	3000 rpm, 100 N	III	II	I
	3000 rpm, 200 N	III	I	II
Thickness	2300 rpm, 100 N	III	I	II
	2300 rpm, 200 N	III	II	I
	3000 rpm, 100 N	II	III	I
	3000 rpm, 200 N	III	II	I
Roughness	2300 rpm, 100 N	II	III	I
	2300 rpm, 200 N	III	II	I
	3000 rpm, 100 N	II	III	I
	3000 rpm, 200 N	I	II	Failure
Deposition Rate	2300 rpm, 100 N	III	II	I
	2300 rpm, 200 N	II	III	I
	3000 rpm, 100 N	I	III	II
	3000 rpm, 200 N	II	I	Failure
Cracks	2300 rpm, 200 N	I	III	II
	3000 rpm, 200 N	II	III	I

I: High, II: Medium, III: Low.

The cross-sectional micrograph of AA2011 coatings fabricated on the substrate exhibited a clear interface with consistent bonding between the deposits and substrate, as presented in Figs. 16 and 17; however, there are several cracks in the deposited coatings. The coating appears to have a consistent thickness and quality, but it was on average the thinnest coating of the three alloys as shown in Fig. 12. One of the small defect sites was studied further by EDS. Uneven distribution of AA2011 alloying elements can be seen in the maps. The EDS maps show a minimal transfer of elements between the tool and substrate, but there seems to be small migration of Ag, Fe, and Mn from the steel to the coating. This phenomenon is also apparent in the EDS maps of the other deposits.

LFS of AA6061 is shown in Figs. 18 and 19. The coating appears to have bonded well to the substrate without cracks. In this approach, there is no sign of plasticization effects in the substrate and intermixing between the consumable material and substrate due to the generated heat; however, intermixing and diffusion across the interface was reported in the conventional FS technique [55]. The EDS maps also show broad regions containing high amounts of Fe in the AA6061 indicating that the substrate surface was rubbed off, and the material was transferred from the substrate to the deposit. These appear to be grains containing Iron along the coating that could possibly have an effect on the strength and roughness.

In the SEM analysis of AA7075 deposits, cracks and unbonded regions at the coatings and substrate interface were observed, as presented in Figs. 20 and 21. This can be explained by the low ductility of AA7075 as compared to the other alloys. The EDS maps revealed the existence of a uniform distribution of oxygen element in the majority of Al-rich regions, which indicates the formation of aluminum oxide after polishing the samples. Moreover, Fe-rich regions in the AA7075 deposits fabricated by higher rotational speed were observed which is proof that the substrate surface was rubbed off during the process due to the high tool rotational speed and force at the tool/substrate interface, and the material was transferred from the substrate to the deposits. The SEM results of all samples do not show elemental diffusion of consumable materials to the substrate or deformation of the substrate, which indicates that the process temperature was low enough to avoid plasticizing the substrate and penetration of the aluminum into the steel substrate.

In order to provide an overview of this study, the results of various analyses employed in this investigation are summarized in Table 6, in which the consumable materials are ranked based on their performances in different examinations. This table summarizes the general trends of high force ratio and lower cracking for AA6061, high thickness, surface roughness, and deposition rate for AA7075, and AA2011 not exhibiting relative high or low values for any measure as predicted by the intermediate values of material properties. Also, there are more results such as EDS maps exhibiting the presence and distribution of elements that cannot be quantified and ranked in this table.

4. Conclusions

A complete analysis of material transfer of AA2011, AA6061, and AA7075 onto AISI 1018 carbon steel by LFS was presented. The results of the experimental study exhibited that the LFS is capable of fabricating the aluminum alloys with great coverage; however, the limitations in the values of process parameters should be considered like any other manufacturing processes. The important process factors such as spindle speed and normal force were considered as the process variables while the traverse speed was kept constant. The influence of different sets of material and process factors on the force ratio, surface roughness, process temperature, material deposition rate, coating coverage, coating thickness, and distribution of elements are discussed in detail. Despite all these analyses, there are still many unknowns about different aspects of the novel method of LFS, such as wear and corrosion performance, residual stress, and temperature distribution in the consumable rod and deposit, which require much more experimental analysis and accurate finite element modeling. The most important outcomes of this investigation are concluded as follows:

- The LFS of three different aluminum alloys resulted in ultra-smooth and thin deposit layers. It was exhibited that AA7075 fabricates thicker and rougher coating layers compared to other alloys in most of the experimental tests, while LFS of AA2011 and AA6061 resulted in the thinnest and smoothest deposits layers, respectively. Moreover, smoother surfaces were obtained by increasing the normal force.
- In this investigation, the force ratio was the highest for AA6061 for all employed parameters, exhibiting a higher friction coefficient for this alloy during the process. Moreover, the highest process temperature was recorded during LFS of this alloy. However, the process temperature generated in LFS is quite low compared to the conventional FS technique, which helps to decrease the thermal effects on the mechanical and metallurgical properties of the deposit.
- The normal force and tool rotational speed are the critical controlling parameters to adjust the input energy into the process. Therefore, increasing the input energy by adopting higher forces, higher rotational speeds, and rougher surfaces may lead to deposition of materials with higher melting points. Lower thermal conductivity and melting point associated with AA7075 resulted in softening the consumable material and failure when the high tool rotational speed and force were employed. The normal applied force was found to have a more significant influence on the process temperature compared to the tool rotational speed.
- The SEM analysis of the cross-sections exhibited a clear interface without any unbonded regions between AA2011 and AA6061 deposits and the substrate; however, cracks and unbonded regions at the interface of AA7075 deposit and the substrate were observed. The SEM results of all samples revealed a defect-free interface with no elemental diffusion of consumable materials to the substrate, which indicates that the LFS process temperature was low enough to avoid plasticizing the substrate and intermixing between the consumable material and substrate.
- The EDS analysis revealed material transferring from the substrate to the coating in most of the samples, indicating that the substrate surface was rubbed off during the process due to high tool speed and force at the tool/substrate interface.

Declaration of Competing Interest

The authors declare that they have no known competing financial interests or personal relationships that could have appeared to influence the work reported in this paper.

Acknowledgments

This investigation was supported by NSF CMMI grant # 1763147 and General Motors.

REFERENCES

[1] Seidi E, Miller SF, Carlson BE. Friction surfacing deposition by consumable tools. J Manuf Sci Eng 2021;143(12):120801.
[2] Gandra J, Krohn H, Miranda RM, Vilaça P, Quintino L, Dos Santos JF. Friction surfacing—a review. J Mater Process Technol 2014;214(5):1062–93.
[3] Seidi E, Miller SF. Friction surfacing using consumable tools: a review. In: Proceedings of the ASME 2019 14th international manufacturing science and engineering conference, vol. 2; 2019. Processes; Materials, V002T03A048.
[4] Gandra J, Pereira D, Miranda RM, Vilaça P. Influence of process parameters in the friction surfacing of AA 6082-T6 over AA 2024-T3. Procedia CIRP 2013;7:341–6.
[5] Kumar BV, Reddy GM, Mohandas T. Influence of process parameters on physical dimensions of AA6063 aluminium alloy coating on mild steel in friction surfacing. Defence Technology 2015;11(3):275–81.
[6] Li H, Qin W, Galloway A, Toumpis A. Friction surfacing of aluminium alloy 5083 on DH36 steel plate. Metals 2019;9(4):479.
[7] Sahoo DK, Mohanty BS. Evaluation of bond strength on deposition of aluminium 6063 alloy over EN24 Medium carbon steel by friction surfacing using different mechtrode diameter. e-J Surf Sci Nanotechnol 2019;17:83–94.
[8] Vitanov VI, Voutchkov II. Process parameters selection for friction surfacing applications using intelligent decision support. J Mater Process Technol 2005;159(1):27–32.
[9] Sahoo DK, Mohanty BS, Pradeep AM, John ADF. An experimental study on friction surfaced coating of Aluminium 6063 over AISI 316 stainless steel substrate. Mater Today: Proceedings 2021;40(1):10–8.
[10] Tokisue H, Katoh K, Asahina T, Usiyama T. Mechanical properties of 5052/2017 dissimilar aluminum alloys deposit by friction surfacing. Mater Trans 2006;47(3):874–82.
[11] Sahoo DK, Mohanty BS, Maalika Veetil AP. Evaluation of bond strength and flash mass on friction surfaced deposition of aluminium 6063 over IS 2062 low carbon steel using different mechtrode face. Ann Chimie Sci Matériaux 2020;44(2):109–19.
[12] Kumar VA, Sammaiah P. Comparison of process parameters influence on mechanical and metallurgical properties of zinc coating on mild steel and aluminium during mechanical process. Material Today Proceedings 2018;5(2):3861–6.
[13] Batchelor AW, Jana S, Koh CP, Tan CS. The effect of metal type and multi-layering on friction surfacing. J Mater Process Technol 1996;57(1–2):172–81.

[14] Chandrasekaran M, Batchelor AW, Jana S. Friction surfacing of metal coatings on steel and aluminum substrate. J Mater Process Technol 1997;72(3):446–52.

[15] Rao KP, Sreenu AV, Rafi HK, Libin MN, Balasubramaniam K. Tool steel and copper coatings by friction surfacing–A thermography study. J Mater Process Technol 2012;212(2):402–7.

[16] Govardhan D, Kumar ACS, Murti KGK, Reddy GM. Characterization of austenitic stainless steel friction surfaced deposit over low carbon steel. Mater Des 2012;36:206–14.

[17] Kramer de Macedo ML, Pinheiro GA, dos Santos JF, Strohaecker TR. Deposit by friction surfacing and its applications. Weld Int 2010;24(6):422–31.

[18] Silva KHS, Brito PP, Santos IB, Câmara MA, Abrão AM. The behaviour of AISI 4340 steel coatings on low carbon steel substrate produced by friction surfacing. Surf Coating Technol 2020;399:126170.

[19] Kallien Z, Rath L, Roos A, Klusemann B. Experimentally established correlation of friction surfacing process temperature and deposit geometry. Surface and Coatings Technology; 2020. p. 126040.

[20] Fitseva V, Hanke S, dos Santos JF, Stemmer P, Gleising B. The role of process temperature and rotational speed in the microstructure evolution of Ti-6Al-4V friction surfacing coatings. Mater Des 2016;110:112–23.

[21] Bararpour SM, Aval HJ, Jamaati R. An experimental and theoretical investigation of thermo-mechanical issues in friction surfacing of Al–Mg aluminum alloys: material flow and residual stress. Model Simulat Mater Sci Eng 2020;28(3). 035003.

[22] Dovzhenko G, Hanke S, Staron P, Maawad E, Schreyer A, Horstmann M. Residual stresses and fatigue crack growth in friction surfacing coated Ti-6Al-4V sheets. J Mater Process Technol 2018;262:104–10.

[23] Troysi F, Silva K, Santos ÍD, Brito P. Investigation of austenitic stainless steel coatings on mild steel produced by friction surfacing using a conventional CNC machining center. Mater Res 2019;22(2). e20180301.

[24] Hanke S, Fischer A, dos Santos JF. Sliding wear behaviour of a Cr-base alloy after microstructure alterations induced by friction surfacing. Wear 2015;338:332–8.

[25] Pereira D, Gandra J, Pamies-Teixeira J, Miranda RM, Vilaça P. Wear behaviour of steel coatings produced by friction surfacing. J Mater Process Technol 2014;214(12):2858–68.

[26] Galvis JC, Oliveira PHF, Martins JDP, Carvalho ALMD. Assessment of process parameters by friction surfacing on the double layer deposition. Mater Res 2018;21(3). e20180051.

[27] Huang YX, Han B, Lv SX, Feng JC, Liu HJ, Leng JS, et al. Interface behaviours and mechanical properties of filling friction stir weld joining AA 2219. Sci Technol Weld Join 2012;17(3):225–30.

[28] Han B, Huang Y, Lv S, Wan L, Feng J, Fu G. AA7075 bit for repairing AA2219 keyhole by filling friction stir welding. Mater Des 2013;51:25–33.

[29] Vasanth R, Mohan K, Rengarajan S, Jayaprakash R, Kumar RA. Characterization and corrosion effects of Friction surfaced IS-2062 E250 CU with AA6063. Mater Res Express 2019;6(12):126579.

[30] Sudherson DPS, Anandkumar PP, Jinu GR, Balasubramanian KA, Vettivel SC. Experimental investigation on corrosion behavior of friction surfaced mild steel with aluminum alloy 5083-Cadmium composite. Mater Res Express 2019;6(8). 086587.

[31] Singh AK, Reddy GM, Rao KS. Pitting corrosion resistance and bond strength of stainless steel overlay by friction surfacing on high strength low alloy steel. Defence Technology 2015;11(3):299–307.

[32] Stegmüller MJ, Grant RJ, Schindele P. Improvements in the process efficiency and bond strength when friction surfacing stainless steel onto aluminium substrates. Proc IME J Mater Des Appl 2019;233(4):687–98.

[33] Galvis JC, Oliveira PHF, Hupalo MF, Martins JP, Carvalho ALM. Influence of friction surfacing process parameters to deposit AA6351-T6 over AA5052-H32 using conventional milling machine. J Mater Process Technol 2017;245:91–105.

[34] Phillips BJ, Avery DZ, Liu T, Rodriguez OL, Mason CJT, Jordon JB, et al. Microstructure-deformation relationship of additive friction stir-deposition Al–Mg–Si. Materialia 2019;7:100387.

[35] Pirhayati P, Aval HJ. Microstructural characterization and mechanical properties of friction surfaced AA2024– Ag composites. Trans Nonferrous Metals Soc China 2020;30(7):1756–70.

[36] Shariq M, Srivastava M, Tripathi R, Chattopadhyaya S, Dixit AR. Feasibility study of friction surfaced coatings over non-ferrous substrates. Procedia Engineering 2016;149:465–71.

[37] Rafi HK, Ram GJ, Phanikumar G, Rao KP. Friction surfaced tool steel (H13) coatings on low carbon steel: a study on the effects of process parameters on coating characteristics and integrity. Surf Coating Technol 2010;205(1):232–42.

[38] Kumar BV, Reddy GM, Mohandas T. Identification of suitable process parameters for friction surfacing of mild steel with AA6063 aluminium alloy. Int J Adv Manuf Technol 2014;74(1–4):433–43.

[39] Murugan CBK, Balusamy V, Padmanaban R, Vignesh RV. Friction surfacing mild-steel with Monel and predicting the coating parameters using fuzzy logic. Mater Today: Proceedings 2018;5(8):16402–10.

[40] Sahoo DK, Chari AN, Reddy AS. Optimization & characterization of friction surfaced coatings of AA6063 aluminium alloy over AISI316 stainless steel substrate. Mater Today: Proceedings 2019;23(3):565–72.

[41] Guo D, Kwok CT, Chan SLI. Spindle speed in friction surfacing of 316L stainless steel–How it affects the microstructure, hardness and pitting corrosion resistance. Surf Coating Technol 2019;361:324–41.

[42] Fitseva V, Krohn H, Hanke S, Dos Santos JF. Friction surfacing of Ti–6Al–4V: process characteristics and deposition behaviour at various rotational speeds. Surf Coating Technol 2015;278:56–63.

[43] Sekharbabu R, Rafi HK, Rao KP. Characterization of D2 tool steel friction surfaced coatings over low carbon steel. Mater Des 2013;50:543–50.

[44] Puli R, Ram GJ. Wear and corrosion performance of AISI 410 martensitic stainless steel coatings produced using friction surfacing and manual metal arc welding. Surf Coating Technol 2012;209:1–7.

[45] Seidi E, Miller SF. A novel approach to friction surfacing: experimental analysis of deposition from radial surface of a consumable tool. Coatings 2020;10(11):1016.

[46] Seidi E, Miller SF. Characterization of lateral friction surfaced AA6063 coatings. In: International mechanical engineering congress and exposition; 2021.

[47] Seidi E, Miller SF. Friction surfacing from radial surface of A6063 aluminum alloy consumable tool onto A36 carbon steel. In: Proceedings of the ASME 2020 international mechanical engineering congress and exposition, vol. 2A; 2020. Advanced Manufacturing, Virtual, Online, V02AT02A003.

[48] Relue W, Seidi E, Hihara LH, Miller SF. Corrosion performance of different aluminum alloy deposits fabricated by lateral friction surfacing. In: International mechanical engineering congress and exposition; 2021.

[49] MatWeb. Online Materials Information Resource. Available from: www.matweb.com. [Accessed 23 March 2021].

[50] Lambiase F, Paoletti A, Di Ilio A. Forces and temperature variation during friction stir welding of aluminum alloy AA6082-T6. Int J Adv Manuf Technol 2018;99(1):337–46.

[51] Chang YP, Huang ZW, Chou HM. Effects of doping elements on the friction and wear of SUJ2 steel sliding against aluminum alloys. Micromachines 2017;8(4):96.

[52] Özler L, Tosun G, Özcan ME. Influence of B4C powder reinforcement on coating structure, microhardness and wear in friction surfacing. Mater Manuf Process 2020;35(10):1135–45.

[53] Tosun G, Ozler L, Ozcan ME. Gradient composite coatings on AA5754 using friction stir process. Surf Eng 2020;36(5):447–55.

[54] Gandra J, Miranda RM, Vilaça P. Performance analysis of friction surfacing. J Mater Process Technol 2012;212(8):1676–86.

[55] Kumar R, Chattopadhyaya S, Ghosh A, Krolczyk GM, Santos Vilaca da Silva P, Kumar R, et al. Characterization of friction surfaced coatings of aisi 316 tool over high-speed-steel substrate. Trans FAMENA 2017;41(2):61–76.